Constraints on primordial black holes and curvature perturbations from the global 21-cm signal

Yupeng Yang●

School of Physics and Physical Engineering, Qufu Normal University, Qufu, Shandong 273165, China;
Collage of Physics and Electrical Engineering, Anyang Normal University, Anyang, Henan 455000, China;
and Joint Center for Particle, Nuclear Physics and Cosmology, Nanjing, Jiangsu 210093, China

The recent observations of the global 21-cm signal by EDGES and gravitational waves by LIGO/ VIRGO have revived interest in primordial black holes (PBHs). Motivated by these observations, many previous works focused on PBHs with lifetimes larger than the present age of the Universe. The influence of massive PBHs with $M_{PBH} \sim \mathcal{O}(10^2)M_\odot$ (taking into account radiation from gas accretion onto PBHs) and less massive PBHs with $M_{PBH} \gtrsim 10^{15}$ g (taking into account Hawking radiation) on the intergalactic medium (IGM) have been considered. Different from previous works, we investigate the influence of PBHs on the evolution of the IGM for the mass range 6×10^{13} g $\lesssim M_{PBH} \lesssim 3 \times 10^{14}$ g. Since the lifetime of these PBHs is smaller than the present age of the Universe, they have evaporated by the present day. Due to Hawking radiation, the heating effects of PBHs on the IGM can suppress the absorption amplitude of the global 21-cm signal. In this work, by requiring that the differential brightness temperature of the global 21-cm signal be in the redshift range of $10 \lesssim z \lesssim 30$, i.e., $\delta T_b \lesssim -100$ mK, we obtain upper limits on the initial mass fraction of PBHs. We find that the strongest upper limit is $\beta_{PBH} \sim 2 \times 10^{-30}$. Since the formation of PBHs is related to primordial curvature perturbations, by using the constraints on the initial mass fraction of PBHs we obtain upper limits on the power spectrum of primordial curvature perturbations for the scale range $8.0 \times 10^{15} \lesssim k \lesssim 1.8 \times 10^{16} \mathrm{Mpc}^{-1}$, corresponding to the mass range considered here. We find that the strongest upper limit is $\mathcal{P}_{\mathcal{R}}(k) \sim 0.0046$. By comparing with previous works, we find that for the mass range (or the scale range) investigated in this work the global 21-cm signal or the 21-cm power spectrum should give the strongest upper limits on the initial mass fraction of PBHs and on the power spectrum of primordial curvature perturbations.

I. INTRODUCTION

Primordial black holes (PBHs) can form in the early epoch of the Universe if there are large density perturbations. Depending on their mass, PBHs can emit different particles via Hawking radiation [1–4], which then interact with other particles in the Universe. The evolution of the intergalactic medium (IGM) is changed due to these interactions, and these changes can influence astrophysical observations, e.g., the global 21-cm signal [5,6].

The Experiment to Detect the Global Epoch of Reionization Signature (EDGES) has reported the observation of the global 21-cm signal, which shows an absorption feature with an amplitude of $T_{21} \sim 500$ mK centered at redshift $z \sim 17$ and is about a factor of 2 larger than expected [7]. According to the theory, the global 21-cm signal is controlled by the evolution of the kinetic temperature (T_k), the cosmic microwave background (CMB) thermodynamic temperature (T_{CMB}), and the spin temperature (T_s). One way to explain the large amplitude observed by the EDGES experiment is to require the IGM to be cooler than expected, which could be caused by, e.g., the interactions between dark matter particles and baryons [8]. Another way is to enhance the intensity of the radio background at low frequencies, which can be satisfied by possible radio sources [9,10]. In general, any additional source (e.g., dark matter annihilation or decay) will heat the IGM and increase the kinetic temperature [6,10–16]. In order to be consistent with the observational results of the EDGES experiment, the properties of the dark matter particles should be constrained [6,10,17–21]. As mentioned above, due to Hawking radiation the evolution of the IGM can be influenced by PBHs, and therefore the mass fraction of PBHs can be constrained by the global 21-cm signal [5,6]. In Ref. [6], the authors focused on PBHs in the mass range $M_{PBH} \gtrsim 10^{15}$ g and investigated their influence on the evolution of the IGM. The lifetime of a PBH with a mass $M_{PBH} \gtrsim 10^{15}$ g is longer than the age of the Universe,

and therefore these PBHs have not evaporated by the present day. Taking into account the global 21-cm signal, the authors of Ref. [6] found the upper limits on the present mass fraction of PBHs depending on the masses of PBHs, e.g., $f_{\rm PBH} \sim 10^{-9}$ for $M_{\rm PBH} \sim 10^{15}$ g. Different from Ref. [6], here we focus on PBHs in the mass range 10^{13} g $\lesssim M_{\rm PBH} \lesssim 10^{14}$ g, which have evaporated in the redshift range $6 \lesssim z \lesssim 1100$. In Ref. [22] the authors investigated the influence of PBHs on the evolution of the IGM for a similar mass range and obtained upper limits on the initial mass fraction of PBHs using the *Planck* 2015 data, e.g., $\beta_{\rm PBH} \sim 10^{-28}$ for $M_{\rm PBH} \sim 10^{14}$ g. For other methods and more detailed discussions on the constraints of initial mass fraction of PBHs see, e.g., Ref. [1] and references therein.

PBHs can be used to investigate the relevant issues of the early Universe. For example, the initial mass fraction of PBHs is related to primordial curvature perturbations [23,24]. A nearly scale-invariant spectrum of primordial curvature perturbations has been predicted by many inflation models [25]. The most robust constraints on the power spectrum of primordial curvature perturbations, $\mathcal{P}_{\mathcal{R}}(k)$, are from the observations and studies of the CMB, Lyman-α forest, and large-scale structure [26–28], and these constraints apply on scales $10^{-4} \lesssim k \lesssim 1$ Mpc^{-1} with a nearly invariant value of $\mathcal{P}_{\mathcal{R}}(k) \sim 10^{-9}$. Since PBHs originate from the collapse of early density perturbations they can be used to constrain primordial curvature perturbations. The upper limits on $\mathcal{P}_{\mathcal{R}}(k)$ from research on PBHs apply on for scales $k \lesssim 10^{20}$ Mpc^{-1} and are about ~ 7 orders of magnitude weaker than that from the CMB, Lyman-α forest, and large-scale structure [23,29,30]. For scales in the range $5 \lesssim k \lesssim 10^8$ Mpc^{-1}, the upper limits on $\mathcal{P}_{\mathcal{R}}(k)$ can be obtained from studies on ultracompact dark matter minihalos, and these limits are about ~ 3 orders of magnitude stronger than that from PBHs [31–36]. In Ref. [37], taking into account the Silk damping effects in the early Universe, the authors found an upper limit of $\mathcal{P}_{\mathcal{R}}(k) \sim 0.06$ for the scale range $10^4 \lesssim k \lesssim 10^5$ Mpc^{-1}. Utilizing the *Planck* 2015 data, the authors of Ref. [22] obtained upper limits on $\mathcal{P}_{\mathcal{R}}(k)$ for the scale range $8.9 \times 10^5 \lesssim k \lesssim 2.8 \times 10^{16}$ Mpc^{-1}. In this work, using the upper limits on the initial mass fraction of PBHs obtained from the global 21-cm signal, we obtain upper limits on $\mathcal{P}_{\mathcal{R}}(k)$ for the scale range $8.0 \times 10^{15} \lesssim k \lesssim 1.8 \times 10^{16}$ Mpc^{-1}.

This paper is organized as follows. In Sec. II we discuss the basic properties of PBHs and their effects on the evolution of the IGM due to Hawking radiation. The influence of PBHs on the global 21-cm signal are investigated in Sec. III. We obtain upper limits on the initial mass fraction of PBHs and the power spectrum of the primordial curvature perturbations in Sec. IV. The conclusions and discussions are given in Sec. V.

II. THE INFLUENCE OF PBHs ON THE EVOLUTION OF THE IGM

A. The basic properties of PBHs

In this section we briefly review the basic properties of PBHs. For more detailed discussions see, e.g., Refs. [1–4,29,38] and references therein.

In the early epoch of the Universe, PBHs can form if there are large density perturbations. The needed amplitude of large density perturbations is generally of $\delta\rho/\rho \gtrsim 0.3$ [39]. According to the theory, a PBH can radiate thermally with temperature [1–4,23]

$$T_{\rm PBH} = \frac{1}{8\pi G M_{\rm PBH}} \approx \left(\frac{M_{\rm PBH}}{10^3 \text{ g}}\right)^{-1} \text{ GeV}. \quad (1)$$

The mass of a PBH changes with time due to Hawking radiation. The mass-loss rate of a black hole can be expressed as [23]

$$\frac{{\rm d}M_{\rm BH}}{{\rm d}t} = -5.34 \times 10^{25} f(M_{\rm BH}) \left(\frac{M_{\rm BH}}{\text{g}}\right) \text{ g s}^{-1}, \quad (2)$$

where $f(M_{\rm BH})$ measures the number of particle species that are emitted directly. $f(M_{\rm BH})$ can be calculated exactly [1] and in this work we use the fitted formula used in, e.g., Ref. [40],

$$\begin{aligned}
f(M_{\rm BH}) &= 1.569 + 0.569 e^{\frac{-0.0234}{T_{\rm BH}}} + 3.414 e^{\frac{-0.066}{T_{\rm BH}}} \\
&+ 1.707 e^{\frac{-0.11}{T_{\rm BH}}} + 0.569 e^{\frac{-0.394}{T_{\rm BH}}} \\
&+ 1.707 e^{\frac{-0.413}{T_{\rm BH}}} + 1.707 e^{\frac{-1.17}{T_{\rm BH}}} \\
&+ 1.707 e^{\frac{-22}{T_{\rm BH}}} + 0.963 e^{\frac{-0.1}{T_{\rm BH}}},
\end{aligned} \quad (3)$$

where $T_{\rm BH}$ is determined by Eq. (1). For the mass range considered here, $f(M_{\rm PBH})$ is in the range $2.5 \lesssim f(M_{\rm BH}) \lesssim 6.1$, corresponding to the temperature range 33 MeV $\lesssim$ $T_{\rm PBH} \lesssim 167$ MeV. For this range, pions, muons, quarks (up, down, and strange), and gluons will be emitted [29,41], and hadrons will be produced after the emission of quarks and gluons through the process of fragmentation. In this work, we will investigate the influence of PBHs on the evolution of the IGM. Based on previous works, it has been found that the main influence of PBHs on the IGM is due to electrons, positrons, and photons [5,12]. Therefore, following previous works, we consider electrons, positrons, and photons that are emitted directly by PBHs or produced indirectly through the decay of, e.g., muons, pions, and other hadrons [1,5,6,41].

The lifetime of a PBH with a fixed mass, $\tau_{\rm PBH}$, can be obtained by integrating Eq. (2). One good approximation of the lifetime can be written as [23]

$$\tau_{PBH} \approx 3 \times 10^{14} \left(\frac{M_{PBH}}{10^{14}\,g}\right)^3 f(M_{PBH})^{-1}\,s. \qquad (4)$$

According to Eq. (4), the lifetime of a PBH with mass $M_{PBH} \sim 5 \times 10^{14}$ g is equal to the age of the Universe, $t \sim 13.7$ Gyr [42]. Therefore, for masses $M_{PBH} < 5 \times 10^{14}$ g, PBHs have evaporated by the present day. The final stages of PBHs, e.g., a stable Planck mass relic or a connection to extra dimensions, have been discussed in previous works [43–45]. Following Ref. [5], in this work we assume that the Hawking evaporation stops at the final stages.

B. The evolution of the IGM including PBHs

The particles emitted from PBHs interact those that exist in the Universe. Due to these interactions, the evolution of the IGM is changed. The main influence of the interactions on the IGM are heating, ionization, and excitation [6,10–13,22,46]. For our purposes, the ionization fraction (x_e) and the temperature of the IGM (T_k) are mainly used to study the evolution of the IGM. The evolutions of x_e and T_k with the redshift can be written as [11–13,22]

$$(1+z)\frac{dx_e}{dz} = \frac{1}{H(z)}[R_s(z) - I_s(z) - I_{add}(z)], \qquad (5)$$

$$(1+z)\frac{dT_k}{dz} = \frac{8\sigma_T a_R T_{CMB}^4}{3m_e c H(z)}\frac{x_e}{1+f_{He}+x_e}(T_k - T_{CMB})$$
$$- \frac{2}{3k_B H(z)}\frac{K_{add}}{1+f_{He}+x_e} + T_k, \qquad (6)$$

where $R_s(z)$ is the recombination rate and $I_s(z)$ is the ionization rate caused by the standard sources. I_{add} and K_{add} are the ionization rate and heating rate caused by the additional sources. For our purposes, I_{add} and K_{add} are caused by PBHs, i.e., $I_{add} \equiv I_{PBH}$ and $K_{add} \equiv K_{PBH}$, and they can be written as [6,11–13,22]

$$I_{PBH} = \chi_i f \frac{1}{n_b}\frac{1}{E_0} \times \left.\frac{dE}{dVdt}\right|_{PBH}, \qquad (7)$$

$$K_{PBH} = \chi_h f \frac{1}{n_b} \times \left.\frac{dE}{dVdt}\right|_{PBH}. \qquad (8)$$

The energy injection rate per unit volume due to PBHs can be written as

$$\left.\frac{dE}{dVdt}\right|_{PBH} = \frac{1}{M_{PBH}}\frac{dM_{PBH}}{dt}n_{PBH}(z), \qquad (9)$$

where $n_{PBH}(z)$ is the number density of PBHs at redshift z. The initial mass fraction of PBHs β_{PBH} can be written as [23]

$$\beta_{PBH} \equiv \frac{\rho_{PBH}^i}{\rho_{crit}^i} = \frac{\rho_{PBH}^{eq}}{\rho_{crit}^{eq}}\left(\frac{a_i}{a_{eq}}\right), \qquad (10)$$

where $a = 1/(1+z)$ is the scale factor, and ρ_{PBH}^i (ρ_{PBH}^{eq}) and ρ_{crit}^i (ρ_{crit}^{eq}) are the mass density of PBHs and the critical density of the Universe at the time of PBH formation (matter-radiation equality), respectively. The scale factor is related to the horizon mass M_H as [23]

$$\frac{a_i}{a_{eq}} = \left(\frac{g_\star^{eq}}{g_\star^i}\right)^{1/12}\left(\frac{M_H}{M_H^{eq}}\right)^{1/2}, \qquad (11)$$

where $g_\star^{eq} \approx 3$ and $g_\star^i \approx 100$ are the total number of effectively massless degrees of freedom at the epoch of matter-radiation equality and PBH formation, respectively. With the above equations, the number density of PBHs can be rewritten as[1]

$$n_{PBH}(z) = \beta_{PBH}\left(\frac{1+z}{1+z_{eq}}\right)^3 \frac{\rho_{crit}^{eq}}{M_{PBH}^i}\left(\frac{g_\star^i}{g_\star^{eq}}\right)^{\frac{1}{12}}\left(\frac{M_H^{eq}}{M_H}\right)^{\frac{1}{2}}$$
$$= 1.46 \times 10^{-4}\beta_{PBH}(1+z)^3\left(\frac{M_{PBH}^i}{g}\right)^{-3/2}, \qquad (12)$$

where M_{PBH}^i is the mass of PBH at the formation time and we have used the relations and values $M_H^{eq} = 1.3 \times 10^{49}(\Omega_m h^2)^{-2}$ g, $M_{PBH}^i = f_M M_H$ with $f_M = (1/3)^{3/2}$, $\rho_{crit} = 1.88 \times 10^{-29}\,h^2$ g cm^{-3}, and $z_{eq} = 3403$ [23,42].

In Eqs. (7) and (8) the factor f stands for the energy fraction injected into the IGM due to Hawking radiation and it is a function of redshift [14,16,47–49]. In general, the energy that can be injected into the IGM is mainly caused by electrons and photons [5,12]. $\chi_{i(h)}$ are the fractions of the energy deposited into the IGM for ionization (heating) [5,11–13,49]. According to theories on structure formation, the first stars were able to form once the redshift $z \sim 30$. These stars became the main sources for ionization, and in this work we adopt the model used in Refs. [10,47]. We have modified the public code RECFAST in CAMB[2] to include the influence of PBHs. The evolutions of x_e and T_k are shown in Fig. 1. For this figure, we have set the initial mass fraction of PBHs as $\beta_{PBH} = 10^{-29}$. Due to the influence of PBHs, in general, x_e and T_k are larger than that for the case with no PBHs, which can be seen clearly in Fig. 1, especially after the redshift $z \sim 600$. The details of the evolutions of x_e and T_k are different depending on the mass of PBHs. Since we have assumed that PBHs stop evaporating at the final stage, there are inflections in Fig. 1. For the mass range 0.6×10^{14} g $\lesssim M_{PBH} \lesssim 10^{14}$ g, PBHs evaporate in the redshift range $30 \lesssim z \lesssim 300$. x_e

---

[1]Here we assume a monochromatic mass fraction for PBHs, and we will investigate the extended mass spectrum for PBHs in detail in future work.
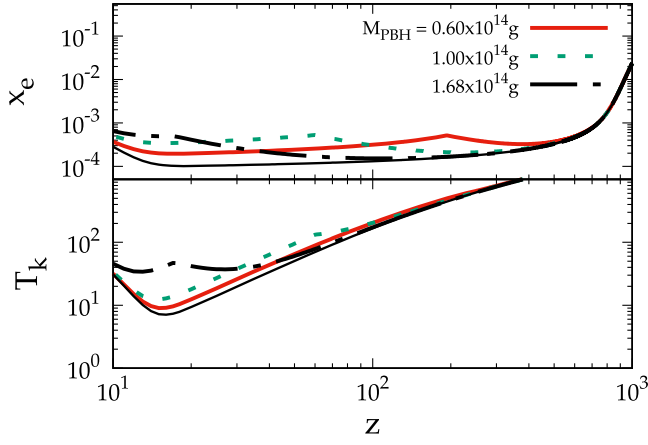[2]https://camb.info/.

FIG. 1. The evolutions of x_e and T_k for different PBH masses: $M_{PBH} = 0.60 \times 10^{14}$ g (red solid line), 1.00×10^{14} g (green dotted line), and 1.68×10^{14} g (black dot-dashed line). Here we have set the initial mass fraction of PBHs as $\beta_{PBH} = 10^{-29}$. For comparison, we also plot the evolutions of x_e and T_k for the case with no PBHs (thin black solid line).

and T_k reach their largest values at the redshift z' (inflections in Fig. 1) corresponding to the lifetime of PBHs. After the redshift z', the evolutions of x_e and T_k tend to follow the cases without PBHs. Similar evolutions can be found for the mass range 10^{14} g $\lesssim M_{PBH} \lesssim 3 \times 10^{14}$ g, in which PBHs evaporate in the redshift range $6 \lesssim z \lesssim 30$.

III. THE INFLUENCE OF PBHs ON THE GLOBAL 21-CM SIGNAL

In the early epoch, the Universe is in the ionized phase and the temperature of the IGM is very high. With the expansion of the Universe, the temperature decreases and hydrogen atoms form due to the combination of protons and electrons at redshift $z \sim 1100$. The 21-cm line is related to the transition between the triplet and singlet levels of the ground state of the hydrogen atom. The transition energy between the two levels is $E = 5.9 \times 10^{-6}$ eV, corresponding to a photon wavelength $\lambda = 21$ cm. The spin temperature T_s, which is used to describe the transition, is defined as [50,51]

$$\frac{n_1}{n_0} = 3 \exp\left(-\frac{T_\star}{T_s}\right), \tag{13}$$

where n_0 and n_1 are the number densities of hydrogen atoms in triplet and singlet states, and $T_\star = 0.068$ K is the temperature corresponding to the transition energy. The spin temperature T_s is mainly effected by (i) background photons, (ii) collisions between hydrogen atoms and other particles, and (iii) resonant scattering of Lyα photons (called the Wouthuysen-Field effect) [50,51]. Considering the cosmic microwave background as the main part of the background photons, the spin temperature can be written as [47,48]

$$T_s = \frac{T_{CMB} + (y_\alpha + y_c)T_k}{1 + y_\alpha + y_c}, \tag{14}$$

where y_α corresponds to the Wouthuysen-Field effect and we adopt the form used in, e.g., Refs. [22,47,52],

$$y_\alpha = \frac{P_{10}T_\star}{A_{10}T_k} e^{-0.3 \times (1+z)^{0.5} T_k^{-2/3} (1+\frac{0.4}{T_k})^{-1}}, \tag{15}$$

where $A_{10} = 2.85 \times 10^{-15}$ s^{-1} is the Einstein coefficient of the hyperfine spontaneous transition. P_{10} is the deexcitation rate of the hyperfine triplet state due to Lyα scattering [50,51]. y_c corresponds to the collisions between hydrogen atoms and other particles [10,47,52–54],

$$y_c = \frac{(C_{HH} + C_{eH} + C_{pH})T_\star}{A_{10}T_k}, \tag{16}$$

where $C_{HH,eH,pH}$ are the deexcitation rates and we adopt the forms used in Refs. [10,52–54].

In general, the differential brightness temperature δT_b is used to describe the global 21-cm signal, which can be written as [10,48,55]

$$\delta T_b = 26(1 - x_e)\left(\frac{\Omega_b h}{0.02}\right)\left[\frac{1+z}{10}\frac{0.3}{\Omega_m}\right]^{\frac{1}{2}}$$

$$\times \left(1 - \frac{T_{CMB}}{T_s}\right) \text{ mK}. \tag{17}$$

Using the above equations, in Fig. 2 we display the evolutions of δT_b in the redshift range $10 \lesssim z \lesssim 300$ for different PBH masses. For comparison, the case with no PBHs is also shown (thin black solid line). From Fig. 2, it
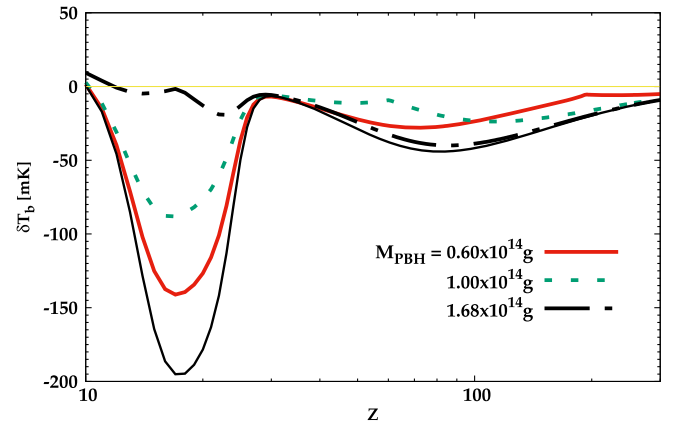

FIG. 2. The evolutions of the differential brightness temperature δT_b in the redshift range $10 \lesssim z \lesssim 300$ for different PBH masses of: $M_{PBH} = 0.60 \times 10^{14}$ g (red solid line), 1.00×10^{14} g (green dotted line), and 1.68×10^{14} g (black dot-dashed line). Here we have set the initial mass fraction of PBHs as $\beta_{PBH} = 10^{-29}$. For comparison, we also plot the evolution of δT_b for the case with no PBHs (thin black solid line).

can be seen that due to the influence of PBHs the absorption amplitude of the global 21-cm signal is suppressed, which is mainly caused by the heating effects of PBHs on the IGM. Similar results can also be found in, e.g., Refs. [5,6,10,47]. Depending on the different PBH masses, the global 21-cm signal exhibits different features and there are also inflections in the plots. For lower mass, e.g., $M_{\rm PBH} = 0.6 \times 10^{14}$ g (red solid line), PBHs evaporate at the redshift $z \sim 200$. For the redshifts $z \lesssim 200$, the evolutions of x_e and T_k (Fig. 1) tend to follow the case with no PBHs but are still larger than that case (thin black solid line). As a result, the amplitude of δT_b becomes smaller than that for the case with no PBHs. For larger mass, e.g., $M_{\rm PBH} = 1.68 \times 10^{14}$ g (black dot-dashed line), PBHs evaporate in the redshift range $10 \lesssim z \lesssim 30$. For this case, the absorption amplitude of the global 21-cm signal is strongly suppressed, and the absorption trough tends to become an emission peak. As shown in Fig. 2, there are two absorption features in the global 21-cm signal. One is in the redshift range $30 \lesssim z \lesssim 300$ and another one appears in the redshift range $10 \lesssim z \lesssim 30$. For the mass range considered here, PBHs have effects on the global 21-cm signal in both redshift ranges. Specifically, the main effects are in the higher (lower) redshift range for the smaller (larger) PBHs depending on their lifetime. For our purposes, inspired by the observational results of the EDGES experiment, we have focused on the redshift range $10 \lesssim z \lesssim 30$. As shown in Fig. 2, for this redshift range larger PBHs have stronger effects on the global 21-cm signal compared with that in the redshift range $30 \lesssim z \lesssim 300$. For the plots, we have set the initial mass fraction of PBHs as $\beta_{\rm PBH} = 10^{-29}$, and PBHs with larger initial mass fractions (fixed mass) should have stronger effects on the global 21-cm signal. Therefore, in view of the observational results of the EDGES experiment, the initial mass fraction of PBHs should have upper bounds, and this issue will be discussed in the following section.

IV. CONSTRAINTS ON PBHs AND CURVATURE PERTURBATIONS

A. Constraints on the initial mass fraction of PBHs

As the discussed above, PBHs with different masses have a different significant influence on the global 21-cm signal. As shown in Fig. 2, the main influence is a suppression of the amplitude of the absorption trough. Moreover, the absorption trough could disappear or become an emission peak due to the effects of PBHs with large initial mass fractions. Therefore, the global 21-cm signal can be used to investigate the abundance of PBHs. Recently, the global 21-cm signal with a large absorption trough was observed by the EDGES experiment at the redshift $z \sim 17$. Following previous works [6,17], we obtain upper limits on the initial mass fraction of PBHs, $\beta_{\rm PBH}$, by requiring the differential brightness temperature of the

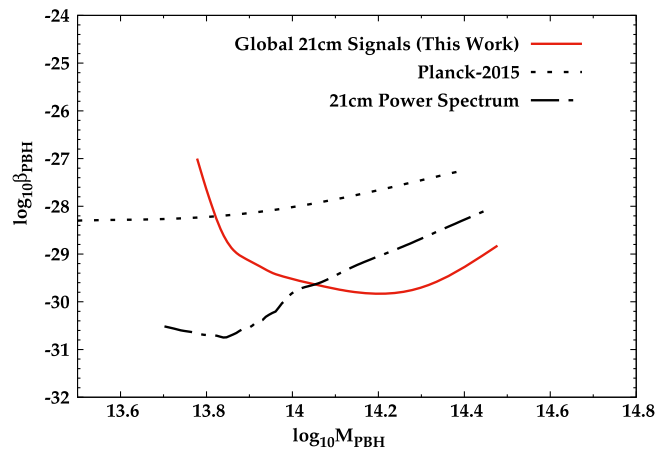
FIG. 3. Constraints on the initial mass fraction of PBHs, $\beta_{\rm PBH}$, by requiring the differential brightness temperature of the global 21-cm signal to be in the redshift range $10 \lesssim z \lesssim 30$ as $\delta T_b \lesssim -100$ mK (red solid line). For comparison, the upper limits from the *Planck* 2015 data [22] (black dotted line) and the potential 21-cm power spectrum [5] (black dashed-dotted line) are also shown.

global 21-cm signal to be $\delta T_b \lesssim -100$ mK. In Fig. 3 we display the upper limits on $\beta_{\rm PBH}$ for the mass range 6×10^{13} g $\lesssim M_{\rm PBH} \lesssim 3 \times 10^{14}$ g (red solid line). From this plot, it can be seen that the strongest upper limit on the initial mass fraction of PBHs is $\beta_{\rm PBH} \sim 2 \times 10^{-30}$. Because we have considered the effects of PBHs on the global 21-cm signal in the redshift range $10 \lesssim z \lesssim 30$, the strongest upper limit appears for larger masses (longer lifetime) in the mass range considered here.

In Ref. [5], using the expected 21-cm power spectrum observed by SKA, the authors obtained potential upper limits on $\beta_{\rm PBH}$ and the strongest upper limit is $\beta_{\rm PBH} \sim 2 \times 10^{31}$, which is also displayed in Fig. 3 (black dashed-dotted line). Different from this work, the authors of Ref. [5] focused on the influence of PBHs on the 21-cm signal in the redshift range $30 \lesssim z \lesssim 300$. Therefore, as shown in Fig. 3, for the mass range considered here the constraints on $\beta_{\rm PBH}$ are stronger for smaller masses (shorter lifetime) than those for larger masses (longer lifetime).

The influence of PBHs on the IGM can also effect the anisotropy of the CMB. Therefore, CMB observations can also be used to investigate the initial mass fraction of PBHs. Utilizing the *Planck* 2015 data, the authors of Ref. [22] obtained upper limits on $\beta_{\rm PBH}$ for the mass range 2.8×10^{13} g $\lesssim M_{\rm PBH} \lesssim 2.5 \times 10^{14}$ g, and they found that the strongest limit is $\beta_{\rm PBH} \sim 4 \times 10^{-29}$ (black dotted line in Fig. 3). Since the constraints on $\beta_{\rm PBH}$ from the CMB data are mainly from the high redshift range, the strongest upper limit on $\beta_{\rm PBH}$ appears for smaller masses,[3] which can be

---

[3]PBHs with smaller masses evaporate before recombination ($z \sim 1000$). Therefore, as shown in Fig. 3, there is a cut on the masses of PBHs.

seen in Fig. 3 and is similar to that of the 21-cm power spectrum.

PBHs with masses $M_{PBH} \lesssim 6 \times 10^{13}$ g evaporate before recombination. Therefore, for this mass range the constraints on the initial mass fraction of PBHs are mainly from big bang nucleosynthesis and CMB distortions [1,40], and the strongest upper limit is about $\beta_{PBH} \sim 10^{-24}$. For large masses $M_{PBH} \gtrsim 6 \times 10^{15}$ g, the constraints on β_{PBH} are mainly from the lensing effect [1]. The radiation from the accretion onto PBHs can also affect the evolution of the IGM, and the CMB data can also be used to obtain upper limits on β_{PBH} [56–59]. The recent observations of gravitational waves provide an important way to constrain the initial mass fraction of PBHs for $M_{PBH} \sim \mathcal{O}(10^2)M_{\odot}$ [60,61]. For other methods and more detailed discussions about the constraints on the initial mass fraction of PBHs see, e.g., Refs. [1,23,62–74] and references therein.

As discussed above, the upper limits of the initial mass fraction of PBHs are different for the different astrophysical observations. Since the main influence of PBHs on the CMB are on the higher redshifts, the upper limit on the initial mass fraction of PBHs with lower mass (shorter lifetime) is stronger than that of PBHs with larger mass. Compared with the smaller mass, as shown in Fig. 2, PBHs with larger mass have a significant influence on the global 21-cm signal observed by the EDGES experiment at redshift $z \sim 17$. Therefore, different from the constraints from the CMB, the upper limit on the initial mass fraction of PBHs with a larger mass (longer lifetime) is stronger than that of PBHs with smaller mass. In particular, PBHs with mass $M_{PBH} \lesssim 10^{13.8}$ g evaporate at redshift $z > 30$. Therefore, the observational results of the EDGES experiment cannot give stringent upper limits on the initial mass fraction of PBHs. On the other hand, since the lifetime of PBHs with mass $M_{PBH} \gtrsim 10^{14.4}$ g is larger than the present age of the Universe, the observational results of the EDGES experiment also cannot give stringent upper limits on the initial mass fraction of PBHs. From Fig. 3, it can be seen that the strongest upper limits correspond to the intermediate mass range, in which PBHs evaporate in the redshift range $10 \lesssim z \lesssim 30$.

Moreover, for the mass range 6×10^{13} g $\lesssim M_{PBH} \lesssim 3 \times 10^{14}$ g, comparing with other constraints, the strongest upper limit on the initial mass fraction of PBHs comes from the observations of the global 21-cm signal or the future 21-cm power spectrum. In this mass range, constraints can also be obtained through studies of the extragalactic photon background, extragalactic antiprotons, and neutrinos [1,29], but the constraints are weaker than the 21-cm constraints [1,5].

B. Constraints on primordial curvature perturbations

PBHs can form via the collapse of the large density perturbations present in the early epoch of the Universe.

The density perturbations can be Gaussian or non-Gaussian [75]. In this work, we have considered Gaussian perturbations, and in this case (in light of the Press-Schechter theory [76]) the initial mass fraction β_{PBH} can be written as [23]

$$\beta_{PBH} = \frac{2M_{PBH}}{M_H} \int_{\delta_c}^{1} p(\delta_H(R)) d\delta_H(R), \qquad (18)$$

where $M_{PBH} = f_M M_H$, M_H is the horizon mass at the formation time of PBHs and f_M is the fraction of the horizon mass that collapses into PBHs. $\delta_c = \delta\rho/\rho$ is the critical value of the density perturbation that can form PBHs, and here we set $\delta_c = 1/3$ [38]. $\delta_H(R)$ is the smoothed density contrast at horizon crossing with $R = (aH)^{-1}$. $p(\delta_H(R))$ is the probability distribution of the smoothed density contrast. For the Gaussian perturbations, $p(\delta_H(R))$ can be written as

$$p(\delta_c(R)) = \frac{1}{\sqrt{2\pi}\delta_H(R)} \exp\left(-\frac{\delta_H^2(R)}{2\sigma_H^2(R)}\right), \qquad (19)$$

where $\sigma_H(R)$ is the mass variance in the form of

$$\sigma^2(R) = \int_0^{\infty} W^2(kR)\mathcal{P}_{\delta}(k) \frac{dk}{k}, \qquad (20)$$

where $W(kR)$ is the Fourier transform of the window function. $\mathcal{P}_{\delta}(k)$ is the power spectrum of the primordial density perturbations, and it is related to the power spectrum of primordial curvature perturbations $\mathcal{P}_{\mathcal{R}}(k)$ as [23]

$$\mathcal{P}_{\delta}(k) = \frac{16}{3}\left(\frac{k}{aH}\right)^2 j_1^2(k/\sqrt{3}aH)\mathcal{P}_{\mathcal{R}}(k), \qquad (21)$$

where j_1 is a spherical Bessel function. Different inflation models predict different forms of $\mathcal{P}_{\mathcal{R}}(k)$. For the general slow-roll inflation models, $\mathcal{P}_{\mathcal{R}}(k)$ can be written as [23,77,78]

$$\mathcal{P}_{\mathcal{R}}(k) = \mathcal{P}_{\mathcal{R}}(k_0)\left(\frac{k}{k_0}\right)^{n(k_0)-1}. \qquad (22)$$

We use this form for our calculations; for more detailed discussions see, e.g., Refs. [23,32,33].

Using the above equations and the constraints on the initial mass fraction of PBHs, in Fig. 4 we display the upper limits on the power spectrum of primordial curvature perturbations for the scale range $8.0 \times 10^{15} \lesssim k \lesssim 1.8 \times 10^{16}$, corresponding to the mass range considered here. The strongest upper limit is $\mathcal{P}_{\mathcal{R}}(k) \sim 0.0046$. For comparison, in Fig. 4 we also display the constraints from the *Planck* 2015 and 21-cm power spectra, corresponding to the constraints on β_{PBH} shown in Fig. 3. Similar to the discussions about the constraints on β_{PBH} in the previous section, for the scale range considered here, since we have focused on the effects of PBHs on the IGM in the redshift range $10 \lesssim z \lesssim 30$, the strongest upper limit appears at the smaller value of $k \sim 1.1 \times 10^{-6}$ Mpc^{-1} with $\mathcal{P}_{\mathcal{R}}(k) \sim 0.0046$,
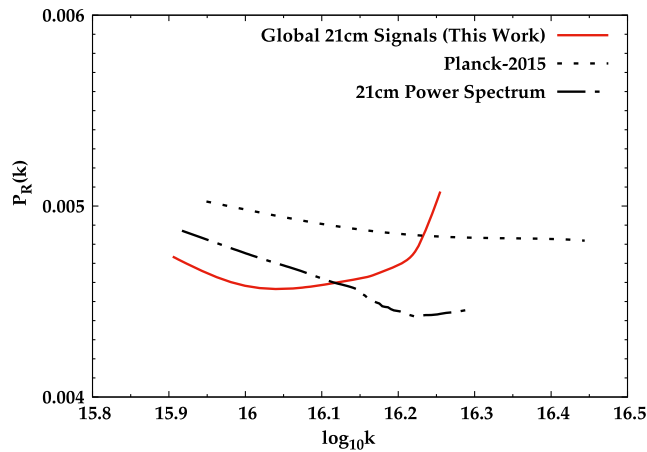
FIG. 4. Constraints on the power spectrum of primordial curvature perturbations, $\mathcal{P}_{\mathcal{R}}(k)$, by requiring the differential brightness temperature of the global 21-cm signal to be in the redshift range $10 \lesssim z \lesssim 30$ as $\delta T_b \lesssim -100$ mK (red solid line). For comparison, the constraints from the *Planck* 2015 data [22] (black dotted line) and the potential 21-cm power spectrum [5] (black dashed-dotted line) are also shown.

corresponding to a larger PBH mass. For the potential constraints from the 21-cm power spectrum, since the authors focused on the redshift range $30 \lesssim z \lesssim 300$, the strongest upper limit appears at the larger value of $k \sim 1.7 \times 10^{-6}$ Mpc^{-1} with $\mathcal{P}_{\mathcal{R}}(k) \sim 0.0044$, which corresponds to a smaller PBH mass. The constraints on $\mathcal{P}_{\mathcal{R}}(k)$ from the CMB are mainly from higher redshifts, and the strongest upper limit appears at the larger value of $k \sim 2.8 \times 10^{-6}$ Mpc^{-1} with $\mathcal{P}_{\mathcal{R}}(k) \sim 0.0048$, corresponding to a smaller PBH mass.

V. CONCLUSIONS

We have investigated the influence of PBHs on the IGM due to Hawking radiation for the mass range 6×10^{13} g $\lesssim M_{PBH} \lesssim 3 \times 10^{14}$ g. Particles emitted by PBHs interact with those that exist in the Universe. Due to these interactions, the degree of ionization and the temperature of the IGM are enhanced after a redshift $z \sim 1100$. The changes of the evolution of the IGM have an influence on astrophysical observations such as the global 21-cm signal. Inspired by the recent observations of the global 21-cm signal in the redshift range $10 \lesssim z \lesssim 30$ by EDGES, we have investigated the effects of PBHs on the global 21-cm signal. We have found that the main effect is to suppress the absorption amplitude of the global 21-cm signal, which is consistent with previous works. By requiring that the differential brightness temperature of the global 21-cm signal be $\delta T_b \lesssim -100$ mK, we obtained upper limits on the initial mass fraction of PBHs depending on their mass. The strongest upper limit is $\beta_{PBH} \sim 2 \times 10^{-30}$. For the mass range of PBHs considered here, the constraints on β_{PBH} can also be obtained using the CMB data, the extragalactic

photon background and the potential 21-cm power spectrum. By comparing these constraints, we found that for the mass range of PBHs considered here the global 21-cm signal or the 21-cm power spectrum could give the strongest upper limit. Since the formation of PBHs is related to primordial curvature perturbations, using the constraints on the initial mass fraction of PBHs we obtained upper limits on the power spectrum of primordial curvature perturbations for the scale range $8.0 \times 10^{15} \lesssim k \lesssim 1.8 \times 10^{16}$ Mpc^{-1}, corresponding to the mass range of PBHs considered here. The strongest upper limit is $\mathcal{P}_{\mathcal{R}}(k) \sim 0.0046$.

Previous works (e.g., Ref. [6]) also investigated the limits on PBHs by requiring $\delta T_b \lesssim -50$ mK. The constraints on the abundance of PBHs are about a factor of 3 weaker for $\delta T_b \lesssim -50$ mK than that of $\delta T_b \lesssim -100$ mK. These differences should have a slight influence on the constraints of primordial curvature perturbations. In this work, inspired by the observational results of EDGES, we focused on the global 21-cm signal in the redshift range $10 \lesssim z \lesssim 30$. As shown in Fig. 2, there are also global 21-cm signals in the redshift range $30 \lesssim z \lesssim 300$, and observing these global 21-cm signals is very difficult. Future experiments that could be run, e.g., on the Moon would detect these global 21-cm signals [79]. As discussed in the above sections and motivated by the work of Ref. [5], the expected 21-cm power spectrum in the redshift range $10 \lesssim z \lesssim 30$ should give stronger upper limits on β_{PBH} or $\mathcal{P}_{\mathcal{R}}(k)$ than that of global 21-cm signals. For the redshift range considered here, the global 21-cm signal can also be influenced significantly by other astrophysical factors, such as the star formation efficiency, the collapse fraction of the halos, and so on [50,51,80]. We will investigate these issues in future work.

In summary, we investigated the influence of PBHs on the global 21-cm signal at the redshift $z \sim 17$ due to Hawking radiation. Compared with previous works, the new features of this work are as follows:

(1) We extended the mass range of PBHs to 6×10^{13} g $\lesssim M_{PBH} \lesssim 3 \times 10^{14}$ g. PBHs with masses in this range evaporate in the redshift range $10 \lesssim z \lesssim 30$, and they are expected to have significant effects on the global 21-cm signal depending on their initial mass fraction β_{PBH}. Inspired by the observational results of the EDGES experiment, by requiring the differential brightness temperature of the global 21-cm signal to be $\delta T_b \lesssim -100$ mK, we have found that the strongest upper limit of the initial mass fraction of PBHs is $\beta_{PBH} \sim 2 \times 10^{-30}$, and as far as we know this is currently the strongest upper limit for the mass range considered here.[4]

---

[4]As shown in Fig. 3, the upper limits from the future expected observations of the power spectrum of the 21-cm signals could be stronger.

(2) Based on the constraints on the initial mass faction of PBHs, we obtained upper limits on the power spectrum of primordial curvature perturbations for the scale range $8.0 \times 10^{15} \lesssim k \lesssim 1.8 \times 10^{16}$ Mpc^{-1}. The strongest upper limit is $\mathcal{P}_{\mathcal{R}}(k) \sim 0.0046$, and this (as far as we know) is currently the best upper limit.

(3) For the mass range considered in this work, and after comparing with other works, we found that the observations and studies on the global 21-cm signal or the power spectrum of the 21-cm signals could give the strongest upper limits on the initial mass fraction of PBHs and the power spectrum of primordial curvature perturbations. Moreover, since the astrophysical influence on the 21-cm signals are very weak in the redshift range $30 \lesssim z \lesssim 300$, future observations of the 21-cm signals in this redshift range (e.g., experiments on the Moon) are very useful for the researches on PBHs.

ACKNOWLEDGMENTS

[1] B. J. Carr, K. Kohri, Y. Sendouda, and J. Yokoyama, Phys. Rev. D **81**, 104019 (2010).
[2] D. N. Page, Phys. Rev. D **16**, 2402 (1977).
[3] D. N. Page, Phys. Rev. D **14**, 3260 (1976).
[4] D. N. Page, Phys. Rev. D **13**, 198 (1976).
[5] K. J. Mack and D. H. Wesley, arXiv:0805.1531.
[6] S. Clark, B. Dutta, Y. Gao, Y.-Z. Ma, and L. E. Strigari, Phys. Rev. D **98**, 043006 (2018).
[7] J. D. Bowman, A. E. E. Rogers, R. A. Monsalve, T. J. Mozdzen, and N. Mahesh, Nature (London) **555**, 67 (2018).
[8] R. Barkana, Nature (London) **555**, 71 (2018).
[9] C. Feng and G. Holder, Astrophys. J. **858**, L17 (2018).
[10] Y. Yang, Phys. Rev. D **98**, 103503 (2018).
[11] Y. Yang, Phys. Rev. D **91**, 083517 (2015).
[12] X. Chen and M. Kamionkowski, Phys. Rev. D **70**, 043502 (2004).
[13] L. Zhang, X. Chen, M. Kamionkowski, Z.-g. Si, and Z. Zheng, Phys. Rev. D **76**, 061301 (2007).
[14] S. Galli, T. R. Slatyer, M. Valdes, and F. Iocco, Phys. Rev. D **88**, 063502 (2013).
[15] J. Chluba, Mon. Not. R. Astron. Soc. **402**, 1195 (2010).
[16] M. S. Madhavacheril, N. Sehgal, and T. R. Slatyer, Phys. Rev. D **89**, 103508 (2014).
[17] G. D'Amico, P. Panci, and A. Strumia, Phys. Rev. Lett. **121**, 011103 (2018).
[18] E. D. Kovetz, I. Cholis, and D. E. Kaplan, Phys. Rev. D **99**, 123511 (2019).
[19] J. R. Bhatt, A. K. Mishra, and A. C. Nayak, Phys. Rev. D **100**, 063539 (2019).
[20] A. Berlin, D. Hooper, G. Krnjaic, and S. D. McDermott, Phys. Rev. Lett. **121**, 011102 (2018).
[21] R. Barkana, N. J. Outmezguine, D. Redigolo, and T. Volansky, Phys. Rev. D **98**, 103005 (2018).
[22] Y. Yang, Mon. Not. R. Astron. Soc. **486**, 4569 (2019).
[23] A. S. Josan, A. M. Green, and K. A. Malik, Phys. Rev. D **79**, 103520 (2009).
[24] G. Sato-Polito, E. D. Kovetz, and M. Kamionkowski, Phys. Rev. D **100**, 063521 (2019).

[25] J. E. Lidsey, A. R. Liddle, E. W. Kolb, E. J. Copeland, T. Barreiro, and M. Abney, Rev. Mod. Phys. **69**, 373 (1997).
[26] R. Hlozek et al., Astrophys. J. **749**, 90 (2012).
[27] S. Bird, H. V. Peiris, M. Viel, and L. Verde, Mon. Not. R. Astron. Soc. **413**, 1717 (2011).
[28] J. L. Tinker, E. S. Sheldon, R. H. Wechsler, M. R. Becker, E. Rozo, Y. Zu, D. H. Weinberg, I. Zehavi, M. R. Blanton, M. T. Busha, and B. P. Koester, Astrophys. J. **745**, 16 (2012).
[29] B. J. Carr, K. Kohri, Y. Sendouda, and J. Yokoyama, Phys. Rev. D **94**, 044029 (2016).
[30] I. Dalianis, J. Cosmol. Astropart. Phys. 08 (2019) 032.
[31] A. S. Josan and A. M. Green, Phys. Rev. D **82**, 083527 (2010).
[32] T. Bringmann, P. Scott, and Y. Akrami, Phys. Rev. D **85**, 125027 (2012).
[33] F. Li, A. L. Erickcek, and N. M. Law, Phys. Rev. D **86**, 043519 (2012).
[34] H. A. Clark, G. F. Lewis, and P. Scott, Mon. Not. R. Astron. Soc. **456**, 1402 (2016); **464**, 955(E) (2017).
[35] Y. Yang, G. Yang, and H. Zong, Phys. Rev. D **87**, 103525 (2013).
[36] Y. Yang, G. Yang, and H. Zong, Europhys. Lett. **101**, 69001 (2013).
[37] D. Jeong, J. Pradler, J. Chluba, and M. Kamionkowski, Phys. Rev. Lett. **113**, 061301 (2014).
[38] B. J. Carr, arXiv:astro-ph/0511743.
[39] A. M. Green and A. R. Liddle, Phys. Rev. D **56**, 6166 (1997).
[40] H. Tashiro and N. Sugiyama, Phys. Rev. D **78**, 023004 (2008).
[41] J. H. Macgibbon and B. R. Webber, Phys. Rev. D **41**, 3052 (1990).
[42] N. Aghanim et al. (Planck Collaboration), arXiv:1807.06209.
[43] M. Kavic, J. H. Simonetti, S. E. Cutchin, S. W. Ellingson, and C. D. Patterson, J. Cosmol. Astropart. Phys. 11 (2008) 017.
[44] M. J. Bowick, S. B. Giddings, J. A. Harvey, G. T. Horowitz, and A. Strominger, Phys. Rev. Lett. **61**, 2823 (1988).
[45] S. R. Coleman, J. Preskill, and F. Wilczek, Mod. Phys. Lett. A **06**, 1631 (1991).

[46] K. M. Belotsky and A. A. Kirillov, J. Cosmol. Astropart. Phys. 01 (2015) 041.

[47] Q. Yuan, B. Yue, X.-J. Bi, X. Chen, and X. Zhang, J. Cosmol. Astropart. Phys. 10 (**2010**) 023.

[48] D. T. Cumberbatch, M. Lattanzi, J. Silk, M. Lattanzi, and J. Silk, Phys. Rev. D **82**, 103508 (2010).

[49] T. R. Slatyer, Phys. Rev. D **93**, 023521 (2016).

[50] J. R. Pritchard and A. Loeb, Rep. Prog. Phys. **75**, 086901 (2012).

[51] S. Furlanetto, S. P. Oh, and F. Briggs, Phys. Rep. **433**, 181 (2006).

[52] M. Kuhlen, P. Madau, and R. Montgomery, Astrophys. J. **637**, L1 (2006).

[53] H. Liszt, Astron. Astrophys. **371**, 698 (2001).

[54] Y. Yang, Eur. Phys. J. Plus **131**, 432 (2016).

[55] B. Ciardi and P. Madau, Astrophys. J. **596**, 1 (2003).

[56] M. Ricotti, J. P. Ostriker, and K. J. Mack, Astrophys. J. **680**, 829 (2008).

[57] L. Chen, Q.-G. Huang, and K. Wang, J. Cosmol. Astropart. Phys. 12 (2016) 044.

[58] Y. Ali-Hamoud and M. Kamionkowski, Phys. Rev. D **95**, 043534 (2017).

[59] V. Poulin, P. D. Serpico, F. Calore, S. Clesse, and K. Kohri, Phys. Rev. D **96**, 083524 (2017).

[60] S. Wang, Y.-F. Wang, Q.-G. Huang, and T. G. F. Li, Phys. Rev. Lett. **120**, 191102 (2018).

[61] S. Bird, I. Cholis, J. B. Muoz, Y. Ali-Hamoud, M. Kamionkowski, E. D. Kovetz, A. Raccanelli, and A. G. Riess, Phys. Rev. Lett. **116**, 201301 (2016).

[62] P. He and L.-Z. Fang, Astrophys. J. **568**, L1 (2002).

[63] A. M. Green, A. R. Liddle, and A. Riotto, Phys. Rev. D **56**, 7559 (1997).

[64] A. Hektor, G. Htsi, L. Marzola, M. Raidal, V. Vaskonen, and H. Veerme, Phys. Rev. D **98**, 023503 (2018).

[65] R. Murgia, G. Scelfo, M. Viel, and A. Raccanelli, Phys. Rev. Lett. **123**, 071102 (2019).

[66] V. B. Petkov, E. V. Bugaev, and P. A. Klimai, arXiv:1912 .01317.

[67] J. Chluba et al., arXiv:1909.01593.

[68] H. Poulter, Y. Ali-Hamoud, J. Hamann, M. White, and A. G. Williams, arXiv:1907.06485.

[69] O. Mena, S. Palomares-Ruiz, P. Villanueva-Domingo, and S. J. Witte, Phys. Rev. D **100**, 043540 (2019).

[70] Y. K. Wang and F. Y. Wang, Astron. Astrophys. **614**, A50 (2018).

[71] T. Nakama, B. Carr, and J. Silk, Phys. Rev. D **97**, 043525 (2018).

[72] Y. Inoue and A. Kusenko, J. Cosmol. Astropart. Phys. 10 (2017) 034.

[73] D. Gaggero, G. Bertone, F. Calore, R. M. T. Connors, M. Lovell, S. Markoff, and E. Storm, Phys. Rev. Lett. **118**, 241101 (2017).

[74] B.-Q. Lu and Y.-L. Wu, Phys. Rev. D **99**, 123023 (2019).

[75] J. C. Hidalgo, arXiv:0708.3875.

[76] W. H. Press and P. Schechter, Astrophys. J. **187**, 425 (1974).

[77] K. Kohri, D. H. Lyth, and A. Melchiorri, J. Cosmol. Astropart. Phys. 04 (2008) 038.

[78] S. M. Leach, I. J. Grivell, and A. R. Liddle, Phys. Rev. D **62**, 043516 (2000).

[79] J. O. Burns, arXiv:2003.06881.

[80] A. Cohen, A. Fialkov, R. Barkana, and M. Lotem, Mon. Not. R. Astron. Soc. **472**, 1915 (2017).